RSC Advances

PAPER

Cite this: *RSC Adv.*, 2016, **6**, 48455

Effect of lanthanum doping on modulating the thermochromic properties of VO_2 thin films

Ning Wang,[a] Nigel Tan Chew Shun,[a] Martial Duchamp,[b] Rafal E. Dunin-Borkowski,[b] Zhong Li[c] and Yi Long*[a]

Received 13th April 2016
Accepted 8th May 2016

DOI: 10.1039/c6ra09514c

www.rsc.org/advances

Lanthanum (La) doped vanadium dioxide (VO_2) thin films were fabricated through a facile sol–gel technique. The La doping was found to be effective for reducing the phase transition temperature (τ_c) of VO_2 below the 4 at% doping level, with a reducing rate of −1.1 °C per at%. In addition, below the 3 at% La doping level, the band gap (E_g) decreased steadily with the increasing addition of La dopants. 5 at% La doping can enhance both the integrated visible transmission (T_{lum}) and the solar modulating ability (ΔT_{sol}) simultaneously. The combination of T_{lum} = 50.1% and ΔT_{sol} = 10.3% represents the best values for VO_2 continuous thin films.

Introduction

Vanadium dioxide (VO_2) is an interesting phase transition material with a critical temperature (τ_c) of around 68 °C, accompanied by a reversible metal to insulator transition (MIT).[1,2] With regards to pure VO_2, the insulating phase (τ_c < 68 °C) with a monoclinic $P2_1/c$ crystal system shows a strong transmission in the infrared (IR)/near infrared (NIR) range, while the metallic counterpart (τ_c > 68 °C) with a tetragonal $P4_2/mnm$ crystal system exhibits depressed transmission across the IR/NIR range.[3,4] The thermal modulating abilities in the IR/NIR range and the electrical conductivity contrast across τ_c make VO_2 a promising candidate for thermochromic smart windows and various smart sensor applications.[5–8] Especially for smart windows, the IR/NIR light can be transmitted ($\tau < \tau_c$) or absorbed ($\tau > \tau_c$) automatically according to the outdoor temperature, maintaining a comfortable indoor environment, which meets today's energy-saving requirements.[9]

However, the high τ_c, low visible transmission (T_{lum}), and low solar modulating abilities (ΔT_{sol}) of pure VO_2 are three main drawbacks to be overcome.[9,10] Moreover, there is always a trade-off between enhancing both T_{lum} and ΔT_{sol} simultaneously.[11] With respect to τ_c, extra strain energy[12] and doping with metal cations with large ionic radii/large valence states[13–15] have proved to be effective in reducing τ_c. As for T_{lum}, the microroughness,[16] widening band gap (E_g),[17] biomimetic nanostructure,[11] nanogrid[7] and porous morphology[18–21] have been reported to be able to increase T_{lum}. Lastly, ΔT_{sol} is always believed to be correlated to the solid contents of VO_2 (ref. 22) and/or surface plasmon resonance (SPR)[10,23] under some special surface/interface conditions.

Rare earth (RE) elements are characterized by their large ionic radii and abundant valence electrons, which always contribute to the enhancement of physical properties as dopants.[24–26] The europium cation (Eu^{3+}) has been found to be effective for reducing the τ_c of VO_2 with a rate of −6.5 °C per at%, and a moderate combination of T_{lum} = 54% and ΔT_{sol} = 6.7% was achieved.[13] The terbium cation (Tb^{3+}) has been reported to be helpful for increasing T_{lum} from ~45% to ~79%, but only a relatively low τ_c reducing rate (−1.5 °C per at%) could be obtained.[27] As predicted by Chao Sun *et al.* using density functional theory (DFT) calculations,[28] doping with the lanthanum cation (La^{3+}) could cause the V–V distance to change and a great V–V dimer distortion, which may result in a decrease in τ_c. In this paper, La^{3+} cations were first experimentally doped into the VO_2 lattice at different doping levels from 1 to 5 at%. It was found that the τ_c of the MIT could be reduced with a rate of −1.1 °C per at%, and a combination of T_{lum} = 50% and ΔT_{sol} = 10.3% could be achieved at the 4 at% doping level.

Experimental section

All of the chemicals – V_2O_5 (99.6%, Alfa Aesar), La_2O_3 (99.9%, Alfa Aesar) and H_2O_2 (30 wt%, Sigma-Aldrich) – were used as received without any further purification.

Precursor preparation

182 mg of V_2O_5 and weighed La_2O_3 powder (0/3.26/6.52/9.78/13.04/16.30 mg) were added into 5 mL of hot H_2O_2 (30 wt%, 90 °C) solution under vigorous stirring. After a violent evaporation and cooling down to room temperature, another 15 mL of H_2O_2 (30 wt%) was added into the suspension, and a clear brown color precursor solution was attained after stirring for 4 minutes. Then the precursor was immediately moved to do the dip coating. It should be noted that the reaction should be done in a 300 mL

[a]School of Materials Science and Engineering, Nanyang Technological University, 50 Nanyang Avenue, 639798, Singapore. E-mail: longyi@ntu.edu.sg
[b]Ernst Ruska-Centre for Microscopy and Spectroscopy with Electrons (ER-C) and Peter Grünberg Institute (PGI), Forschungszentrum Jülich, 52428, Germany
[c]School of Mechanical and Aerospace Engineering, Nanyang Technological University, Nanyang Avenue, 639798 Singapore

beaker due to the strong heat release during the reaction between V_2O_5 and hot H_2O_2.

VO_2 thin film fabrication

A fused silica substrate with dimensions of 15 × 15 × 0.5 mm^3 was dipped into the precursor solution at a rate of 50 mm min^{-1}. After immersing for 20 seconds, the substrate was lifted up vertically at a withdrawing rate of 200 mm min^{-1}. After drying in air, a brownish thin film with a thickness of ~60 nm per side was on the substrate. Then the thin film was moved into a tube furnace and annealed at 550 °C for 2 h in an Ar flow (200 mL min^{-1}).

Characterization

The phase of the products was characterized with a Shimadzu XRD-6000 X-ray diffractometer (Cu-Kα, $\lambda = 0.15406$ nm) using a voltage of 40 kV and a current of 30 mA at an X-ray grazing angle of 1.0°. Their morphology and La doping level were determined using a field emission scanning electron microscope (FESEM, JSM-7600F, JEOL, Japan) with an INCA EDX detector at an accelerating voltage of 5 kV and 20 kV, respectively. For conventional transmission electron microscopy (TEM) studies, *i.e.* using selected area electron diffraction (SAED) and bright field (BF) imaging, a JEOL 2010 (JEOL Company, Japan) microscope was used at an accelerating voltage of 200 kV. Transmittance spectra in the range of 250–2500 nm were measured using an UV-vis-NIR spectrophotometer (Cary 5000, Agilent Ltd, USA) equipped with a Linkam PE120 system Peltier heating & cooling stage. The integrated visible transmittance (T_{lum} 380–780 nm) and solar/IR transmittance (T_{sol} 280–2500 nm; T_{IR} 780–2500 nm) were calculated based on the recorded % T spectra using the expression:

$$T_{lum/sol} = \int \varphi_{lum/sol}(\lambda)T(\lambda)d\lambda \Big/ \int \varphi_{lum/sol}(\lambda)d\lambda \quad (1)$$

where $T(\lambda)$ is the recorded film transmittance, φ_{lum} is the standard luminous efficiency function for the photopic vision of human eyes,[29] and φ_{sol} is the solar irradiance spectrum for air mass 1.5 (corresponding to the sun standing 37° above the horizon).[30] The hysteresis loop of % T at a wavelength of 2000 nm was measured at temperatures ranging from 20 to 100 °C. In order to attain the phase transition temperature τ_c, the temperature-dependent heating and cooling % $T(\tau)$ data were fitted using a sigmoidal function of the form:[31]

$$\%\ T(\tau) = A_2 + (A_1 - A_2)/[1 + \exp(\tau - \tau_c)/B] \quad (2)$$

where τ is the temperature in °C and A_1, A_2, τ_c and B are fitting parameters. Two phase transition temperatures, $\tau_{c,h}$ and $\tau_{c,c}$, were obtained in the heating and cooling cycles, respectively and the average phase transition temperature was defined as: $\tau_c = (\tau_{c,h} + \tau_{c,c})/2$, $\Delta\tau_c = \tau_{c,h} - \tau_{c,c}$. The solar modulating ability is termed as: $\Delta T_{sol} = T_{sol}$ (20 °C) − T_{sol} (90 °C).

Results and discussion

Synthesis of the La doped VO_2 thin films

Fig. 1a shows the XRD patterns of the pristine and La doped VO_2 thin films. The bump around 20° (2θ) in the XRD patterns should be ascribed to the diffraction of the amorphous fused silica substrates. All of the thin films exhibit the characteristic (011) XRD peak of VO_2 (monoclinic, $P2_1/c$, JCPDS #82-661) around 28° (2θ), and no other impurity phase can be found, indicating the successful synthesis of the VO_2 phase. Compared with the pristine VO_2, the (011) peak position in the 5 at% La doped sample is left-shifted by 0.2° from 28.0° to 27.8°, which indicates the lattice expansion arising from the replacement of

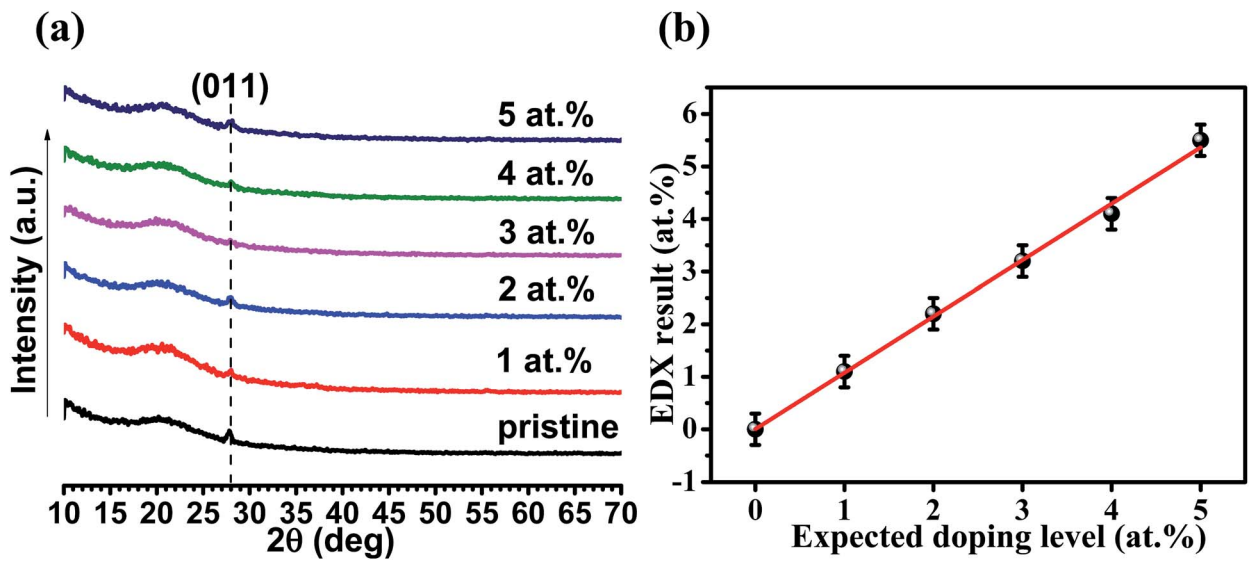

Fig. 1 (a) XRD patterns of the pristine and La doped (1–5 at%) VO_2 thin films. (b) La doping levels determined by EDX characterization with a 10% deviation.

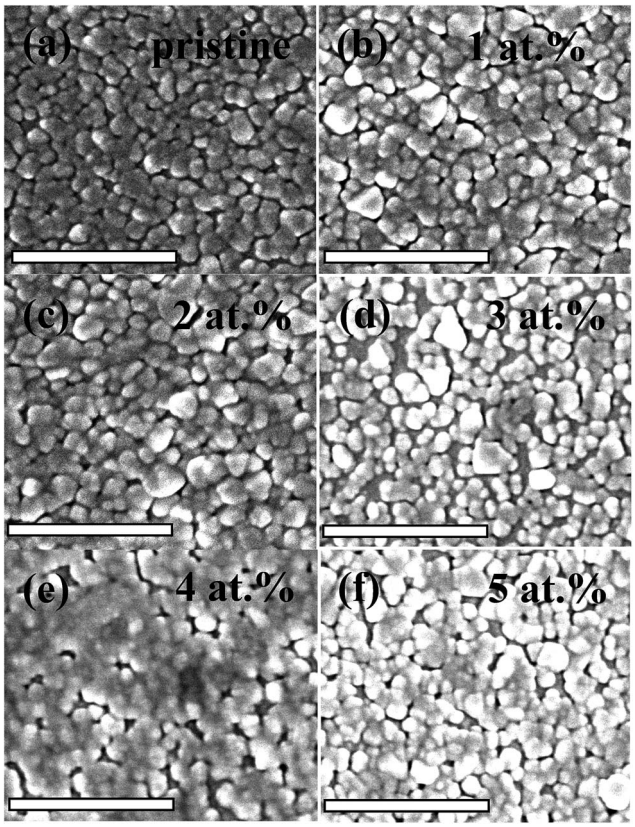

Fig. 2 FESEM images for the pristine (a) and La doped (1–5 at%) (b–f) VO_2 thin films. The scale bars in the images are 500 nm.

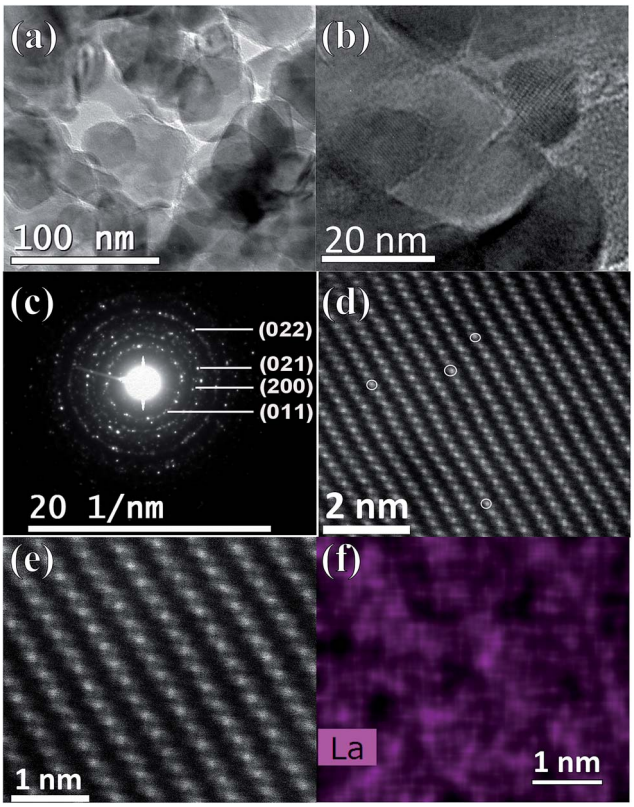

Fig. 3 TEM image (a) and the enlarged TEM image (b) of the 3 at% La doped VO_2 grains. (c) SAED pattern of the polycrystalline 3 at% La doped VO_2 grains. (d) STEM image of the 3 at% La doped VO_2 grains. (e) HAADF image of the doped sample. (f) The La elemental mapping related to (e).

V by La with a relatively larger ionic radius (1.032 Å *vs.* 0.58 Å) in accordance with the DFT calculations.[28] The La doping levels were further confirmed by EDX analysis with a 10% deviation. As depicted in Fig. 1b, the EDX results agree well with the expected doping levels.

Fig. 2 shows the morphology evolution of the pristine and La doped VO_2 thin films tested using FESEM. All of the samples show a nanograin packed morphology, and the average grain size for the 0–5 at% La doped samples is 61, 72, 84, 79, 62 and 73 nm, respectively, which shows that the La doping gives rise to a slight increase in the grain size. The roughness and thickness of the thin films have been detected using AFM under tapping mode, and are tabulated in Table 1. The thickness of the La-doped samples shows a deviation by $\sim\pm14$ nm compared to the pristine VO_2 thin film, while the roughness exhibits a slight increase by 1.1–5.6 nm. The TEM characterization of the 3 at% La doped sample is shown in Fig. 3. As shown in Fig. 3a and b, the bright-field TEM images reveal that the average grain size of the sample is $\sim$80 nm, consistent with the SEM result (Fig. 2). The SAED pattern, as shown in Fig. 3c, exhibits diffraction rings that can be indexed to the (011), (200), (021) and (022) faces of VO_2, which indicates the polycrystalline nature of the La doped VO_2 thin film. The doping of La was further investigated through STEM. As shown in Fig. 3d, the atom replacement of V by La could be clearly observed in the high resolution STEM image, where the La atoms with the larger atomic number are brighter than the V atoms, arising from their different contributions to the elastic scattering signals collected by the detector. In addition, the STEM–EDX elemental mapping (Fig. 3f) related to the view of the HAADF (high angle annular dark field) shows that the La atoms are incorporated into the VO_2 lattice as the distribution of La signals matches the lattice plane arrangement.

Table 1 Thermochromic properties of the La doped VO_2 thin films

Doping level/at%	Thickness/nm	R_a[a]/nm	T_{lum} (20 °C/90 °C)/%	ΔT_{sol}[b]/%	τ_c (heating/cooling)/°C
0	74	3.0	64.8/64.8	7.3	79.9/57.1
1	83	4.4	61.1/61.3	9.1	76.1/52.4
2	60	8.6	67.5/67.7	6.2	79.6/54.2
3	72	4.4	55.8/56.6	8.4	76.2/54.9
4	**90**	**4.1**	**49.9/50.4**	**10.3**	**75.9/49.2**
5	**80**	**5.5**	**69.5/68.9**	**9.0**	**80.2/55.2**

[a] R_a is the average roughness. [b] $\Delta T_{sol} = T_{sol}$ (20 °C) $- T_{sol}$ (90 °C).

Thermochromic properties

Fig. 4a shows the transmittance (% T) spectra ($250 < \lambda < 2500$ nm) of the samples at temperatures of 20 and 90 °C. Upon heating from 20 to 90 °C, a large % T contrast in the IR range could be observed for all of the samples, which should be

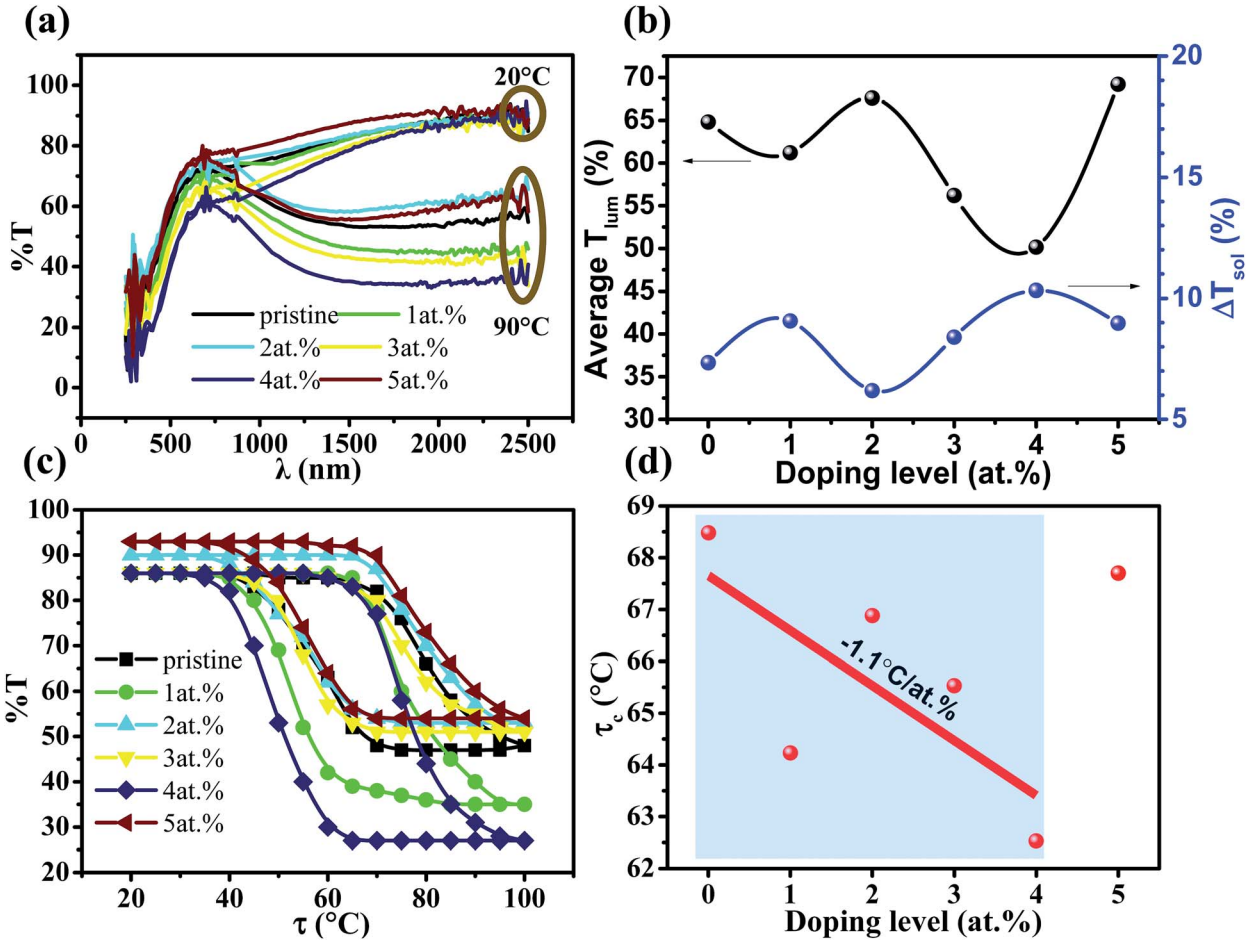

Fig. 4 (a) UV-vis-NIR spectra of the pristine and La doped (1–5 at%) VO_2 thin films at temperatures of 20 and 90 °C. (b) Average T_{lum} and the ΔT_{sol} of the VO_2 thin films with different La doping levels. (c) % *T* hysteresis loop of the pristine and La doped (1–5 at%) VO_2 thin films. (d) Plot of τ_c *vs.* La doping level.

ascribed to the MIT.[20,32,33] The integrated T_{lum} and ΔT_{sol} are tabulated in Table 1, and Fig. 4b shows the doping level dependent average T_{lum} and ΔT_{sol}. It can be observed that the best combination of T_{lum} = 50.1% and ΔT_{sol} = 10.3% was achieved at the La doping level 4 at%, which represents the best value for RE element-doped VO_2 thin films,[13,27,34] and is comparable to other doping cases without RE elements.[35–40] It is of interest that both the average T_{lum} and ΔT_{sol} at the La doping level 5 at% are higher than that of pristine VO_2 (69.2%, 9.0% *vs.* 64.8%, 7.3%), which should be due to a surface plasmon resonance peak around 1250 nm arising from the La doping. The % *T* hysteresis loop was recorded at a wavelength of 2000 nm in the temperature range 20–100 °C. As shown in Fig. 4c, after doping with La, the MIT tends to move towards a lower temperature until the doping level of 4 at%, which is similar to the case with Eu doping.[13] A plot of the doping level dependent τ_c is shown in Fig. 4d, and a τ_c reducing rate of −1.1 °C per at% could be attained below the doping level of 4 at%. This is the first experiment to prove the efficiency of La doping for reducing τ_c as indicated in simulation work using DFT calculations.[28] With respect to the τ_c reduction mechanism, besides the lattice distortion from the substitution of large La atoms calculated by DFT,[28] the increase in the hole carrier density (h^+) from V^{5+} propagating caused by La doping ($V^{4+}{}_{1-2x}V^{5+}{}_xLa^{3+}{}_xO_2$) should also contribute to the adjustment of τ_c.[41] The competition between these two mechanisms should be the reason why τ_c starts to increase at a higher La doping level.

As listed in Table 2, compared to two other reported rare earth dopants Eu^{3+} and Tb^{3+}, the La^{3+} cation has the largest ionic radius. The average T_{lum} of the RE element-doped VO_2 thin films decreases with the ascending ionic radius of the dopant and this is consistent with the fact that larger ions result in greater electronic polarization and slower velocity of light, leading to a larger refractive index. From Tb^{3+} to Eu^{3+} dopants, the ionic radius increases from 0.92 to 0.95 Å and the τ_c reducing rate is increased from 1.5 to 6.5 °C per at%, which should be due to the larger lattice distortion. However, the largest size, La^{3+}, doping shows the lowest τ_c reducing rate and the reason remains unknown, but some dot defects in the form of La insertion in the seriously distorted lattice may be partially attributed to this phenomenon. In addition, compared to the previously reported W-/Mg-doped VO_2 continuous thin films (Table 2), the La-doped thin film shows the best combination of T_{lum} (50.1%) and ΔT_{sol} (10.3%).

Table 2 Doping effects on the thermochromic performance of VO_2 continuous films[a]

Cation	Ionic radius/Å	Doping/at%	Average T_{lum}/%	ΔT_{sol}/%	$d\tau_c$/dat%	Ref.
RE doping						
Eu^{3+}	0.95	4	54	6.7	−6.5	13
Tb^{3+}	0.92	4	65.9	4.6	−1.5	27
La^{3+}	1.03	4	50.1	10.3	−1.1	This work
Other dopings						
W^{6+}	0.6	2	45.1	6.9	20	42
Ti^{4+}	0.605	—	40	4.6	—	43
Mg^{2+}	0.72	5	82.1	4.8	1.4	10

[a] The thickness, roughness and grain size of the RE element-doped VO_2 thin films are at the same level.

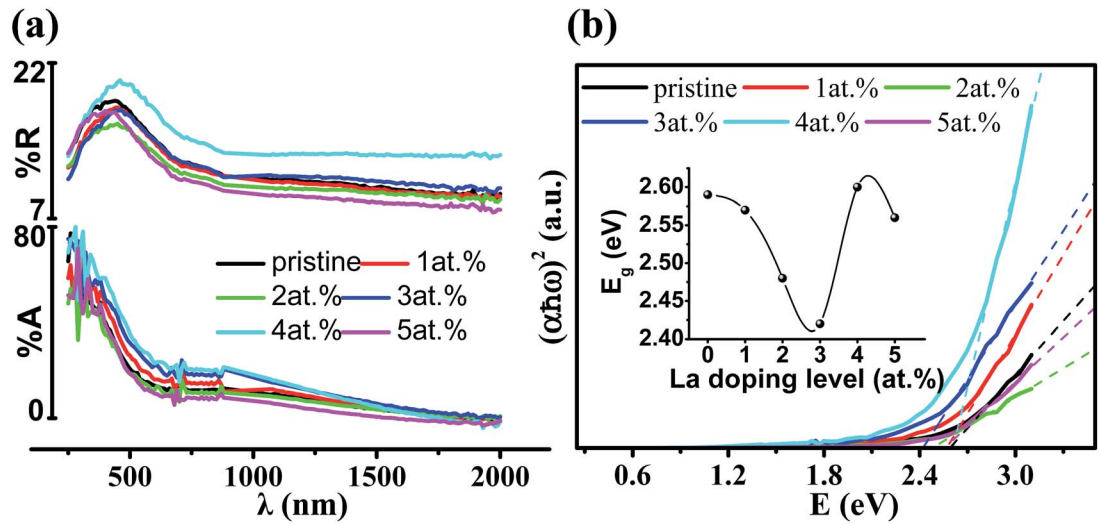

Fig. 5 (a) % *A* and % *R* spectra of the pristine and La doped (1–5 at%) VO_2 thin films at room temperature. (b) Curve of $(\alpha\hbar\omega)^2$ *vs.* *E* and the band gap E_g (inset) with different La doping levels.

Fig. 5a shows the % *A* and % *R* spectra of the pristine and La doped VO_2 thin films. It can be found that the % *A* and % *R* could be changed by La doping, where the 5 at% and 4 at% La doped samples exhibit the lowest and highest % *A*/% *R*, resulting in the highest and lowest % *T*, respectively. In order to further investigate the La doping effects on the optical properties, the direct bandgap (E_g) of the VO_2 thin films was calculated by fitting the linear part of the $(\alpha\hbar\omega)^2$ *vs.* *E* curves (Fig. 5b) based on the equation $(\alpha\hbar\omega)^2 = A(\hbar\omega - E_g)$,[44,45] where α is the absorption coefficient ($\alpha d = -\ln(T/1 - R)$), *A* is a constant, and $\hbar\omega$ is the photon energy. As depicted in the inset of Fig. 5b, the E_g of the VO_2 thin films gradually declines upon doping with La. The lowest value of 2.42 eV is achieved at the doping level of 3 at%, and then it returns back with further doping. The decrease of E_g below the doping level of 3 at% is similar to the case with tungsten (W) doping, which arises from the larger ionic radius,[46] and the following E_g widening should be due to the competition between the effect of the large ionic radius and the h^+ carrier density. Since the change in the band gap is of an electronic nature,[44] the E_g narrowing of the La doped VO_2 thin films below 3 at% doping should be also related to the change in the band structure resulting from the La doping in the lattice.

Conclusions

In summary, a series of La doped VO_2 thin films was prepared through a facile sol–gel method, and the thin films exhibited high visible transmission and large solar modulating abilities. In particular, the 4 at% La doped sample shows the best combination of $T_{lum} = 50.1\%$ and $\Delta T_{sol} = 10.3\%$, compared with other reported VO_2 continuous thin films. Compared with pristine VO_2, the 5 at% La doped sample can increase T_{lum} and ΔT_{sol} simultaneously. La doping was first proved to be able to reduce the τ_c of the MIT in an experiment, which is consistent with the simulation work, and a reducing rate of −1.1 °C per at% is followed below the doping level of 4 at%. A narrowing of the band gap was observed below the doping level of 3 at%, which should be ascribed to the change in the band structure caused by the doping in the VO_2 lattice with large La atoms. This investigation of La doping effects on the thermochromic properties of VO_2 thin films should be useful for other element doping research using elements with a large ionic radius and low valence state.

Acknowledgements

This research was supported by the Singapore National Research Foundation under the CREATE programme: Nanomaterials for Energy and Water Management, Singapore Ministry of Education (MOE) Academic Research Fund Tier 1 RG101/13, JTC-sponsored FYP program AY 2015-16 and an MSE-ERC Julich collaboration-MAP project grant. XRD, FESEM and TEM characterization was performed at the Facility for Analysis, Characterization, Testing and Simulation (FACTS) in Nanyang Technological University, Singapore and in the Ernst Ruska-Centre for Microscopy and Spectroscopy with Electrons (ER-C) in Forschungszentrum Jülich, Germany. The authors acknowledge financial support from the European Union under the Seventh Framework Programme under a contract for an Integrated Infrastructure Initiative. Reference 312483 – ESTEEM2. One of the authors, Nigel Tan Chew Shun, thanks the NTU-JTC Industrial Infrastructure Innovation Centre Singapore for their support.

Notes and references

1 R. Heckingbottom and J. W. Linnett, *Nature*, 1962, **194**, 678.
2 F. Morin, *Phys. Rev. Lett.*, 1959, **3**, 34–36.
3 M. E. A. Warwick and R. Binions, *J. Mater. Chem. A*, 2014, **2**, 3275–3292.
4 Y. Gao, H. Luo, Z. Zhang, L. Kang, Z. Chen, J. Du, M. Kanehira and C. Cao, *Nano Energy*, 2012, **1**, 221–246.
5 M. Kamalisarvestani, R. Saidur, S. Mekhilef and F. S. Javadi, *Renewable Sustainable Energy Rev.*, 2013, **26**, 353–364.
6 A. K. Prasad, S. Amirthapandian, S. Dhara, S. Dash, N. Murali and A. K. Tyagi, *Sens. Actuators, B*, 2014, **191**, 252–256.
7 C. Liu, I. Balin, S. Magdassi, I. Abdulhalim and Y. Long, *Opt. Express*, 2015, **23**, A124–A132.
8 B. Hu, Y. Ding, W. Chen, D. Kulkarni, Y. Shen, V. V. Tsukruk and Z. L. Wang, *Adv. Mater.*, 2010, **22**, 5134–5139.
9 C. Wu and Y. Xie, *Energy Environ. Sci.*, 2010, **3**, 1191–1206.
10 N. Wang, S. Liu, X. T. Zeng, S. Magdassi and Y. Long, *J. Mater. Chem. C*, 2015, **3**, 6771–6777.
11 X. Qian, N. Wang, Y. Li, J. Zhang, Z. Xu and Y. Long, *Langmuir*, 2014, **30**, 10766–10771.
12 J. Cao, E. Ertekin, V. Srinivasan, W. Fan, S. Huang, H. Zheng, J. W. L. Yim, D. R. Khanal, D. F. Ogletree, J. C. Grossmanan and J. Wu, *Nat. Nanotechnol.*, 2009, **4**, 732–737.
13 X. Cao, N. Wang, S. Magdassi, D. Mandler and Y. Long, *Sci. Adv. Mater.*, 2014, **6**, 558–561.
14 A. Romanyuk, R. Steiner, L. Marot and P. Oelhafen, *Sol. Energy Mater. Sol. Cells*, 2007, **91**, 1831–1835.
15 T. D. Manning, I. P. Parkin, C. Blackman and U. Qureshi, *J. Mater. Chem.*, 2005, **15**, 4560–4566.
16 J. Du, Y. Gao, Z. Chen, L. Kang, Z. Zhang and H. Luo, *Sol. Energy Mater. Sol. Cells*, 2013, **110**, 1–7.
17 S.-Y. Li, N. R. Mlyuka, D. Primetzhofer, A. Hallén, G. Possnert, G. A. Niklasson and C. G. Granqvist, *Appl. Phys. Lett.*, 2013, **103**, 161907.
18 X. Cao, N. Wang, J. Y. Law, S. C. J. Loo, S. Magdassi and Y. Long, *Langmuir*, 2014, **30**, 1710–1715.
19 M. Zhou, J. Bao, M. Tao, R. Zhu, Y. Lin, X. Zhang and Y. Xie, *Chem. Commun.*, 2013, **49**, 6021–6023.
20 N. Wang, Y. Huang, S. Magdassi, D. Mandler, H. Liu and Y. Long, *RSC Adv.*, 2013, **3**, 7124–7128.
21 L. Kang, Y. Gao, H. Luo, Z. Chen, J. Du and Z. Zhang, *ACS Appl. Mater. Interfaces*, 2011, **3**, 135–138.
22 A. Taylor, I. Parkin, N. Noor, C. Tummeltshammer, M. S. Brown and I. Papakonstantinou, *Opt. Express*, 2013, **21**, A750–A764.
23 Y. Zhou, A. Huang, Y. Li, S. Ji, Y. Gao and P. Jin, *Nanoscale*, 2013, **5**, 9208–9213.
24 X. Yuan, Y. Sun and M. Xu, *J. Solid State Chem.*, 2012, **196**, 362–366.
25 Y. Tian, J. Zhang, X. Jing and S. Xu, *Spectrochim. Acta, Part A*, 2012, **98**, 355–358.
26 R. Sagar, P. Hudge, S. Madolappa, A. C. Kumbharkhane and R. L. Raibagkar, *J. Alloys Compd.*, 2012, **537**, 197–202.
27 N. Wang, M. Duchamp, R. E. Dunin-Borkowski, S. Liu, X. Zeng, X. Cao and Y. Long, *Langmuir*, 2016, **32**, 759–764.
28 C. Sun, L. Yan, B. Yue, H. Liu and Y. Gao, *J. Mater. Chem. C*, 2014, **2**, 9283–9293.
29 G. Wyszecki and W. S. Stiles, *Color Science: Concepts and Methods, Quantitative Data and Formulae*, Wiley, New York, 2nd edn, 2000.
30 *ASTM G173-03 Standard Tables of Reference Solar Spectral Irradiances: Direct Normal and Hemispherical on a 37° Tilted Surface*, Annual Book of ASTM Standards American Society for Testing and Materials, Philadelphia, PA, USA, 2003, vol. 14.04, http://rredc.nrel.gov/solar/spectra/am1.5.
31 G. Beydaghyan, V. Basque and P. V. Ashrit, *Thin Solid Films*, 2012, **522**, 204–207.
32 N. Wang, S. Magdassi, D. Mandler and Y. Long, *Thin Solid Films*, 2013, **534**, 594–598.
33 C. Liu, N. Wang and Y. Long, *Appl. Surf. Sci.*, 2013, **283**, 222–226.
34 L. Song, Y. Zhang, W. Huang, Q. Shi, D. Li, Y. Zhang and Y. Xu, *Mater. Res. Bull.*, 2013, **48**, 2268–2271.
35 Y. Xu, W. Huang, Q. Shi, Y. Zhang, L. Song and Y. Zhang, *J. Sol-Gel Sci. Technol.*, 2012, **64**, 493–499.
36 Y. Jiazhen, Z. Yue, H. Wanxia and T. Mingjin, *Thin Solid Films*, 2008, **516**, 8554–8558.
37 J. Zhang, H. He, Y. Xie and B. Pan, *J. Chem. Phys.*, 2013, **138**, 114705–114706.
38 J. Zhou, Y. Gao, X. Liu, Z. Chen, L. Dai, C. Cao, H. Luo, M. Kanahira, C. Sun and L. Yan, *Phys. Chem. Chem. Phys.*, 2013, **15**, 7505–7511.
39 Y. F. Gao, C. X. Cao, L. Dai, H. J. Luo, M. Kanehira, Y. Ding and Z. L. Wang, *Energy Environ. Sci.*, 2012, **5**, 8708–8715.
40 D. Li, M. Li, J. Pan, Y. Luo, H. Wu, Y. Zhang and G. Li, *ACS Appl. Mater. Interfaces*, 2014, **6**, 6555–6561.
41 J. Wei, Z. Wang, W. Chen and D. H. Cobden, *Nat. Nanotechnol.*, 2009, **4**, 420–424.
42 L. T. Hu, H. Z. Tao, G. H. Chen, R. K. Pan, M. N. Wan, D. H. Xiong and X. J. Zhao, *J. Sol-Gel Sci. Technol.*, 2016, **77**, 85–93.
43 W. L. Hu, G. Xu, J. W. Ma, B. Xiong and J. F. Shi, *Acta Phys.-Chim. Sin.*, 2012, **28**, 1533–1538.

44 S. Hu, S. Y. Li, R. Ahuja, C. G. Granqvist, K. Hermansson, G. A. Niklasson and R. H. Scheicher, *Appl. Phys. Lett.*, 2012, **101**, 201902.
45 G.-H. Liu, X.-Y. Deng and R. Wen, *J. Mater. Sci.*, 2010, **45**, 3270–3275.
46 M. K. Dietrich, B. G. Kramm, M. Becker, B. K. Meyer, A. Polity and P. J. Klar, *J. Appl. Phys.*, 2015, **117**, 185301.